Incorporation of Inhomogeneous Ion Diffusion Coefficients into Kinetic Lattice Grand Canonical Monte Carlo Simulations and Application to Ion Current Calculations in a Simple Model Ion Channel†

Hyonseok Hwang*

Department of Chemistry, Kangwon National University, Chuncheon, Kangwon 200-701, Republic of Korea

George C. Schatz and Mark A. Ratner

Department of Chemistry, Northwestern University, 2145 Sheridan Rd., Evanston, Illinois 60208-3113

Received: July 24, 2007; In Final Form: September 20, 2007

To deal with inhomogeneous diffusion coefficients of ions without altering the lattice spacing in the kinetic lattice grand canonical Monte Carlo (KLGCMC) simulation, an algorithm that incorporates diffusion coefficient variation into move probabilities is proposed and implemented into KLGCMC calculations. Using this algorithm, the KLGCMC simulation method is applied to the calculation of ion currents in a simple model ion channel system. Comparisons of ion currents and ion concentrations from these simulations with Poisson−Nernst−Planck (PNP) results show good agreement between the two methods for parameters where the latter method is expected to be accurate.

I. Introduction

Kinetic or dynamic lattice Monte Carlo (KLMC or DLMC) simulation algorithms[1−4] and Brownian dynamics (BD) simulation methods[5−8] are useful tools for studying ion transport in complex systems such as an ion channel.[9−12] The molecular dynamics (MD) simulation method,[13−16] which can describe ion transport at an atomistic level, is computationally too demanding to reach the time scales needed for ion transport in ion channels. On the other hand, Poisson−Nernst−Planck (PNP) theory,[17−20] based on a dielectric continuum model, can be used to calculate ion currents at necessary time scales, but several important issues such as finite ion size and correlation effects are ignored in that theory. As alternative computational methods, the KLMC and BD simulation methods overcome limitations of both MD and PNP methods by using a simple description of the proteins and membranes and employing explicit ions. Consequently, KLMC simulations and BD simulations can be performed for time scales relevant to ion transport in ion channels.

In a lattice-based approach, the ions move on a fixed lattice for each time step. Consequently, when ions have a spatially varying diffusion coefficient such as occurs inside a channel,[6,15] the implementation of an inhomogeneous diffusion coefficient into a lattice-based method causes difficulty.

Cheng et al. proposed a method to incorporate the inhomogeneous diffusion coefficients of ions into DLMC simulations.[3] In that method, the lattice spacing is varied depending on the diffusion coefficients, and the electrostatic interaction energies at the ion positions are calculated with a multilinear interpolation algorithm. This use of interpolation is a computational limitation for this method.

Natori and Godby and later Righi et al. have shown a linear relationship between the time and the mean square displacement of an adatom on a surface when the diffusion coefficient has an Arrhenius form.[21,22] Oum and co-workers revealed that when the diffusion coefficient is expressed in terms of the sojourn time of a particle at a position it is equivalent to the Arrhenius form.[23] Farnell and Gibson performed off-lattice Monte Carlo (MC) simulations of diffusion with a spatially varying diffusion coefficient, and showed that accurate results can be produced by altering both the MC step size and the stepping probability.[24]

In this paper, we introduce a probability-based algorithm to deal with inhomogeneous diffusion coefficients of ions without altering the lattice spacing and implement this algorithm into a kinetic lattice grand canonical Monte Carlo (KLGCMC) simulation method, a lattice-based simulation approach. By maintaining a constant lattice spacing, this algorithm does not require any interpolation scheme and is easy to implement into a lattice-based method. We also calculate ion currents in a simple model ion channel using this probability-based KLGCMC algorithm.

This probability-based algorithm is basically the same as other kinetic Monte Carlo (KMC) schemes proposed by Gillespie[25] or by Fichthorn and Weinberg[26] in that all of them describe the stochastic processes of multiple events, but those KMC schemes are used to simulate the reaction process while the algorithm in this paper is used to describe the diffusion process of ions.

This paper is organized as follows. In the next section, the probability-based algorithm to treat inhomogeneous diffusion coefficients of ions is proposed. A simple model system is introduced, and applications of the KLGCMC simulation method from Hwang et al.[4] with this algorithm to the model system are presented in section III. Comparisons of KLGCMC simulation results with PNP calculations are also made in the same section. Further studies of the KLGCMC simulation method with the probability-based algorithm are discussed in the final section.

† Part of the "Giacinto Scoles Festschrift".

* To whom correspondence should be addressed. E-mail: hhwang@kangwon.ac.kr.

10.1021/jp075838o CCC: $37.00
Published on Web 10/26/2007

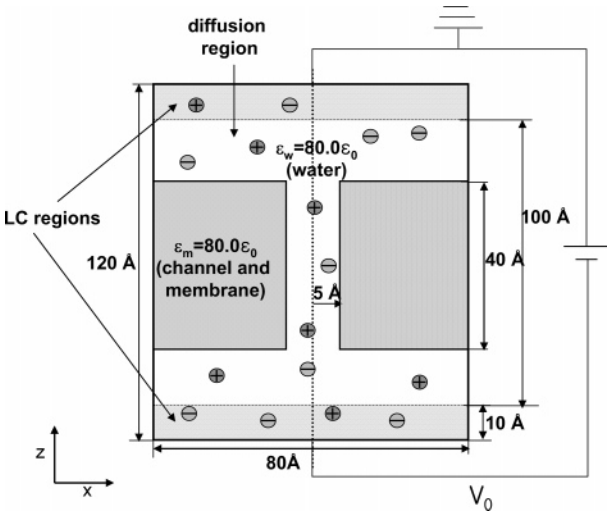

Figure 1. 2D cross section of a 3D model ion channel system. The local control regions in the KLGCMC are located at the bottom ($-60 \le z < -50$ Å) and the top ($50 < z \le 60$ Å). $L_z^{\text{diff}} = 100$ Å and $L_{\text{chn}} = 40$ Å. The bulk salt concentration at both LC regions is 0.1 M.

II. Methods

A. Kinetic Lattice Grand Canonical Monte Carlo (KLGCMC) Simulations with the Local Control Method. Because the details of the KLGCMC simulation with the local control method are discussed elsewhere,[4,27−30] we only briefly describe the simulation method here. In this method, the creation and deletion of ions are restricted to local control (LC) regions, and only diffusion occurs in the diffusion region. For the ion channel in this work, the LC regions are located at the bottom and top of the simulation box shown in Figure 1.

In this simulation method, ion creation is performed by randomly selecting a lattice site in one of the two LC regions and by attempting to create a cation or anion on that lattice point. A creation attempt is accepted or rejected with a probability, $P_{N_L \to N_L+1}$):

$$P_{N_L \to N_L+1} = \min\left\{1, \frac{\rho_v}{N_N + 1} \exp[B - \beta(U_{N_L+1} - U_{N_L} - q_{\text{cre}}\phi_{\text{cre}}(\mathbf{r}_{\text{cre}}))]\right\} \quad (1)$$

where $\rho_v \equiv V_L/V$ where V_L and V are the volumes of a local control region and the simulation box, respectively. In eq 1, N_L (or $N_L + 1$) is the ion number in that local control region before (or after) an attempt, U_{NL} (or $U_{N_L} + 1$) is the total interaction energy of ions before (or after) an attempt, q_{cre} and $\mathbf{r}_{\text{cre}}$ are the charge and position of the created ion, $\phi_{\text{ext}}(\mathbf{r})$ is an external field explained later, and β is $1/k_BT$ where k_B is the Boltzmann constant and T is a temperature. The constant B in eq 1 is given as

$$B \equiv \beta\mu + \ln\frac{V}{\Lambda^3} \quad (2)$$

where μ is the chemical potential of the created ion and $\Lambda \equiv h/(2\pi m k_B T)^{1/2}$ where m is the mass of the created ion. In the applications in this paper, we assume that cations and anions have the same chemical potential and mass.

For ion deletion, an ion in one of the two LC regions is randomly selected and an attempt to delete that ion is accepted or rejected by generating and comparing a random number with a probability, $P_{N_L \to N_L-1}$):

$$P_{N_L \to N_L-1} = \min\left\{1, \frac{N_L}{\rho_v} \exp[-B - \beta(U_{N_L-1} - U_{N_L} + q_{\text{del}}\phi_{\text{ext}}(\mathbf{r}_{\text{del}}))]\right\} \quad (3)$$

where q_{del} and $\mathbf{r}_{\text{del}}$ are the charge and position of the deleted ion.

An ion move is performed by sequentially selecting an ion and moving it to one of the six nearest-neighbor sites in the case of 3D. The move is accepted or rejected with a probability, $P_{a \to b}$ given by

$$P_{a \to b} = \min\{1, \exp[-\beta(U_{N_b} - U_{N_a})]\} \quad (4)$$

where U_{N_a} (or U_{N_b}) is the total interaction energy before (or after) a move and a (or b) is the ion position before (or after) a move.

A time step, which is required to calculate ion currents, is given as[4]

$$\Delta t = \frac{(\Delta L)^2}{6D^{\text{ref}}} \quad (5)$$

where ΔL is the lattice spacing in the KLGCMC simulation and D^{ref} is a reference ion diffusion coefficient, which will be explained in the next subsection. Then, ion currents are calculated using the equation

$$I_{\text{ion}} = \frac{\langle N_{\text{ion}}^{\text{cross}} \rangle}{\Delta t} = \frac{6D\langle N_{\text{ion}}^{\text{cross}} \rangle}{(\Delta L)^2} \quad (6)$$

where $N_{\text{ion}}^{\text{cross}}$ is the number of ions (cations or anions) crossing the cross section per time step.

B. Implementation of Inhomogeneous Diffusion Coefficients. In the KLGCMC simulation, a constant lattice spacing is employed in all regions of the simulation box. To treat inhomogeneous ion diffusion coefficients without altering the lattice spacing, we introduce an algorithm based on move probability.

Natori and Godby[21] and later Righi et al.[22] showed a linear relationship between time and mean square displacement when the ratio of two diffusion coefficients is written as

$$\frac{D_i(\mathbf{r}_i)}{D^{\text{ref}}} = \exp\left[-\frac{E_i^{\text{act}}(\mathbf{r}_i)}{k_BT}\right] \quad (7)$$

where $D_i(\mathbf{r}_i)$ and $E_i^{\text{act}}(\mathbf{r}_i)$ are a space-dependent diffusion coefficient and an activation barrier energy of ion i at $\mathbf{r}_i$. The reference diffusion coefficient D^{ref} is chosen as the largest value among the bulk diffusion coefficients of the cation and anion. Oum et al. showed that when the ratio of two different diffusion coefficients of ion i is written as

$$\frac{D_i(\mathbf{r}_i)}{D^{\text{ref}}} = \frac{1}{\tau_i(\mathbf{r}_i)} \quad (8)$$

then eq 8 is equivalent to eq 7.[23] In eq 8, $\tau_i(\mathbf{r}_i)$ is a dimensionless sojourn time of ion i at $\mathbf{r}_i$. We now introduce a diffusion probability of ion i as

$$P_i^{\text{dif}}(\mathbf{r}_i) \equiv \frac{1}{\tau_i(\mathbf{r}_i)} = \frac{D_i(\mathbf{r}_i)}{D^{\text{ref}}} \quad (9)$$

where it is assumed that $D^{ref} \geq D_i(\mathbf{r}_i)$. Equation 9 implies that the ion i moves to one of the nearest-neighbor lattices with a probability of $P_i^{dif}(\mathbf{r}_i) = 1/\tau_i(\mathbf{r}_i)$ when the ion diffusion coefficient is smaller than D^{ref} but moves unconditionally when the diffusion coefficient is D^{ref}. Thus to make a move attempt for ion i due to the diffusion coefficient $D_i(\mathbf{r})$, a random number is generated and compared with the diffusion probability $P_i^{dif}(\mathbf{r})$ from eq 9.

C. Interaction Energy Calculation. To test the proposed KLGCMC simulation method and the algorithm for implementing inhomogeneous ion diffusion coefficients, we consider a problem with very simple interactions. First of all, no electrostatic interaction between ions is assumed and ions only interact with an applied external field. A hard-sphere potential between ions is employed as a short range interaction. Second, we assume the dielectric constants of the channel and the membrane to be the same as the water dielectric constant $80\epsilon_0$ to avoid any reaction field effect. Then, the total interaction energy U_N in the system can be written as[1,31,32]

$$U_N(\mathbf{r}_1,\mathbf{r}_2,\cdots,\mathbf{r}_N) = \sum_{i<j} u_{ij}(\mathbf{r}_i,\mathbf{r}_j) + \sum_i h_i(\mathbf{r}_i) + \sum_i q_i\phi_{ext}(\mathbf{r}_i) - k_B T \sum_i \ln\left[\frac{D_i(\mathbf{r}_i)}{D^{ref}}\right] \quad (10)$$

Here the direct interaction between ions i and j, $u_{ij}(\mathbf{r}_i,\mathbf{r}_j)$ is a hard-sphere potential given as

$$u_{ij}(\mathbf{r}_i,\mathbf{r}_j) = \begin{cases} \infty & |\mathbf{r}_i - \mathbf{r}_j| < \sigma_i + \sigma_j \\ 0 & \text{otherwise} \end{cases} \quad (11)$$

where σ_i and σ_j is the radii of the ions i and j, respectively. The interaction energy $h_i(\mathbf{r})$ in the second term represents the hard-wall interaction of ion i with the boundaries between water and the channel or membrane region and is given by

$$h_i(\mathbf{r}_i) = \begin{cases} \infty & \mathbf{r}_i \in \text{channel or membrane region} \\ 0 & \text{otherwise} \end{cases} \quad (12)$$

We assume the external field $\phi_{ext}(\mathbf{r})$ to be linear and expressed as

$$\phi_{ext}(\mathbf{r}) = V_0 \frac{L_z^{dif}/2 - z}{L_z^{dif}} \quad (13)$$

where L_z^{dif} is the length of the diffusion region along the z axis and V_0 is a voltage applied to the bottom of the model ion channel system (see Figure 1).

To describe inhomogeneous diffusion in the KLGCMC simulation correctly, the diffusion probability $P_i^{dif}(\mathbf{r}_i)$ in (9) must be taken into account in the interaction energy$U_N(\mathbf{r}_1,\mathbf{r}_2,\cdots,\mathbf{r}_N)$. The last term in eq 10 incorporates this diffusion probability into the KLGCMC simulation.[3,6,24]

III. Data and Results

A. Description of the Model System and Details of KLGCMC Simulations. A 2D cross section of the 3D model ion channel system under investigation is shown in Figure 1. The model ion channel is depicted as a cylinder whose radius and length are 5 and 40 Å, respectively. The LC regions are located at the bottom ($-60 \leq z < -50$ Å) and the top ($50 < z \leq 60$ Å) of the system. The length of the diffusion region in the z direction L_z^{dif} is set as 100 Å. For simplicity, no fixed charges are introduced inside the ion channel and a linear external voltage in eq 13 is applied to the system. To avoid the reaction field effect due to the dielectric boundaries, dielectric constants of the channel and membrane are assumed to be $80\epsilon_0$.

TABLE 1: Ion Parameters

ions	charge (e)	radii (Å)	D^{blk} (10^{-5} cm^2/s)	**B** (eq 2) 0.10 M
cation	+1	1.0	2.0	4.54
anion	−1	1.0	2.0	4.54

We use a small ion radius of 1.0 Å for both cations and anions to reduce finite ion size effect.[20] The parameter B in eq 2, associated with the bulk salt concentration, is determined by performing LGCMC simulations for a bulk ion system with different B values and by selecting a value that gives the bulk salt concentration of 0.1 M.[4] The bulk concentration of 0.1 M is used for all the simulations in this work. See Table 1 for the ion parameters used in the simulations.

KLGCMC simulations are performed on a 81 × 81 × 121 grid with a grid size of 1.0 Å. Periodic boundary conditions are used in the x and y directions, whereas a reflecting boundary condition is used in the z direction. To calibrate the present results, we also use PNP theory to calculate current−voltage curves and other properties.[18,20] PNP is a dielectric continuum model which should lead to the same results for our assumed ion channel parameters as long as reaction field effects are not important. The PNP calculations are carried out on a 81 × 81 × 101 grid with a grid size of 1.0 Å to have the same resolution as the KLGCMC simulations. To define the ion-accessible region inside the channel, a Stern layer parameter of 1.0 Å is used for the PNP calculations.[32] For calculating ion currents at each applied voltage, the data are collected for 9 000 000 KLGCMC cycles after 1 000 000 KLGCMC cycles are completed to define a steady-state.

B. Discontinuously Changing Diffusion Coefficients inside the Channel. In this section, we present a case where the diffusion coefficients of ions change discontinuously inside the channel. In this case, the diffusion coefficient, $D(\mathbf{r})$ in eq 9 is given as

$$D_{cat(or\ ani)}^{dis}(\mathbf{r}) = \begin{cases} D^{chn} & |z| < L_{chn}/2 \\ D^{blk} & \text{otherwise} \end{cases} \quad (14)$$

where $L_{chn} = 40$ Å is the length of the channel and $D^{chn} = 2.0$, 1.0, and 0.5×10^{-5} cm^2/s, respectively (see Figure 2). In this example we assume that the diffusion coefficients of the cation and anion are the same. D^{ref} is taken to be $D^{ref} = D^{blk} = 2.0 \times 10^{-5}$ cm^2/s.

Figure 3 shows the dependence of the cation current density−voltage curves on the inside-channel diffusion coefficients. Since the channel has no ion selectivity, the cation and anion current densities are the same and for clarity, and only the cation current densities are presented. As expected, decrease of the inside-channel diffusion coefficient of the cation leads to a decrease in the cation current density. Good agreement between the KLGCMC simulation results and the PNP calculations is seen in Figure 3.

The ion concentrations at $V_0 = -0.2$ V are presented in Figure 4. At $V_0 = -0.2$ V, cations flow from the top to the bottom of the simulation box, and anions flow in the opposite direction. As the inside-channel ion diffusion coefficient decreases, the ion concentration in the channel increases because the slow transport of the ions leads to pile-up of the ions inside the channel. The average numbers of the cations and anions inside the channel are (0.686, 0.686), (0.762, 0.783), and (0.824, 0.838)

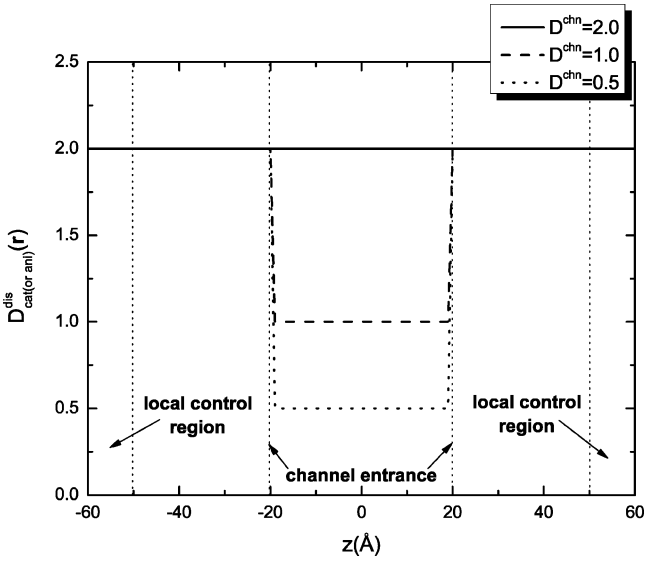

Figure 2. Discontinuously changing diffusion coefficients of ions as a function of *z*. The cation and anion are assumed to have the same bulk and inside-channel diffusion coefficients. The locations of the channel entrances at $z = \pm 20$ Å and the local control regions at $z = \pm 50$ Å are also shown. The diffusion coefficients are in units of 10^{-5} cm^2/s.

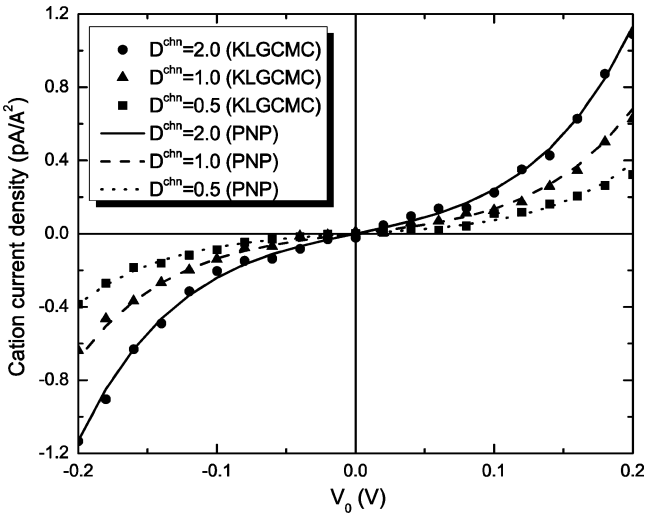

Figure 3. Dependence of cation current density−voltage curves on the inside-channel diffusion coefficients in the case of discontinuously changing diffusion coefficients. Comparison between the KLGCMC simulation results and the PNP calculations is also shown. For clarity, only the cation current densities are presented. The bulk salt concentration is 0.1 M. The diffusion coefficients (see inset) are in units of 10^{-5} cm^2/s.

in panels a−c of Figure 4, respectively. Good agreement between the KLGCMC simulation results and the PNP calculations is shown.

C. Continuously Changing Diffusion Coefficients inside the Channel. In this section, we present another case where the diffusion coefficients of ions continuously change inside the channel. The diffusion coefficient $D(\mathbf{r})$ in eq 9 is given as a function of *z* as follows:[6]

$$D^{\mathrm{con}}_{\mathrm{cat(or\ ani)}}(\mathbf{r}) = \begin{cases} D^{\mathrm{chn}} & |z| < 10\ \text{Å} \\ D^{\mathrm{chn}} + (D^{\mathrm{chn}} - D^{\mathrm{blk}})f(z) & 10\ \text{Å} \le |z| < L_{\mathrm{chn}}/2 \\ D^{\mathrm{blk}} & \text{otherwise} \end{cases}$$

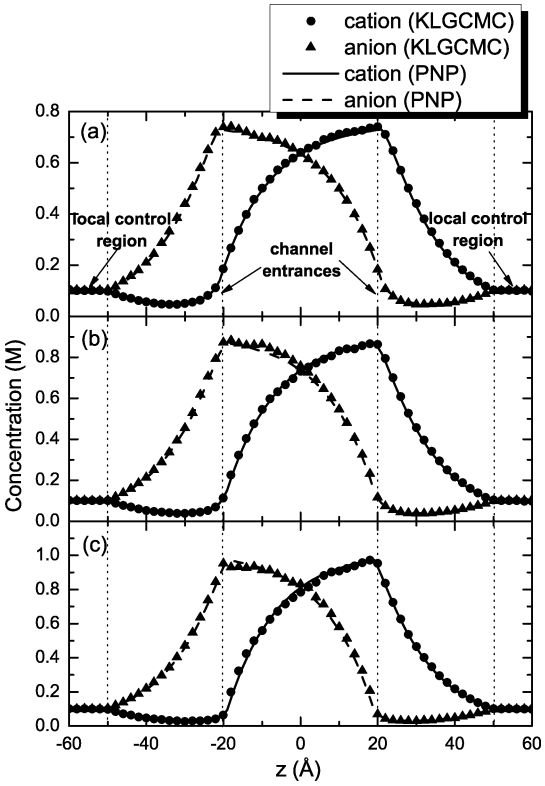

Figure 4. Dependence of cation and anion concentration profiles on the inside-channel ion diffusion coefficients at $V_0 = -0.2$ V. (a) $D^{\mathrm{chn}} = 2.0 \times 10^{-5}$ cm^2/s, (b) $D^{\mathrm{chn}} = 1.0 \times 10^{-5}$ cm^2/s, and (c) $D^{\mathrm{chn}} = 0.5 \times 10^{-5}$ cm^2/s. Comparison between the KLGCMC simulation results and the PNP calculations is also presented. The locations of the channel entrances at $z = \pm 20$ Å and the local control regions at $z = \pm 50$ Å are also shown. The bulk salt concentration in both LC regions is 0.1 M.

where $f(z) = 2((z - z_c)/L_c)^3 - 3((z - z_c)/L_c)^2$ and $z_c = 10$ Å and $L_c = L_{\mathrm{chn}}/2 - z_c$ and $D_{\mathrm{chn}} = 2.0$, 1.0, and 0.5×10^{-5} cm^2/s, respectively. As in the previous example, the diffusion coefficients of the cation and anion in bulk and inside the channel are assumed to be the same. Then $D^{\mathrm{ref}} = D^{\mathrm{blk}} = 2.0 \times 10^{-5}$ cm^2/s. The $D(\mathbf{r})$ is shown in Figure 5.

The dependence of the cation current density−voltage curves on the inside-channel diffusion coefficients is shown in Figure 6. As in the previous case, only the cation current densities are presented for clarity. Good agreement between the KLGCMC simulation results and the PNP calculations is also found in Figure 6.

Figure 7 shows the ion concentrations at $V_0 = -0.2$ V. The average numbers of the cations and anions inside the channel are (0.686, 0.686), (0.822, 0.817), and (0.938, 0.912) in panels a−c of Figure 7, respectively. Compared with the previous case, the ion concentrations in this case increase inside the channel and have a maximum around $z = \pm z_c$. This leads to a higher average number of ions in the channel. Good agreement between the KLGCMC simulation results and the PNP calculations is also shown in Figure 7.

D. Asymmetric Diffusion Coefficients of Cations and Anions in Bulk as well as inside the Channel. In this example, cations and anions have asymmetric diffusion coefficients in both baths as well as inside the channel. That is, the ion diffusion coefficients of cations and anions at the bottom of the system and in the lower part of the channel are different from those at the top of the system and in the upper part of the channel. The space-dependent cation and anion diffusion coefficients are given as

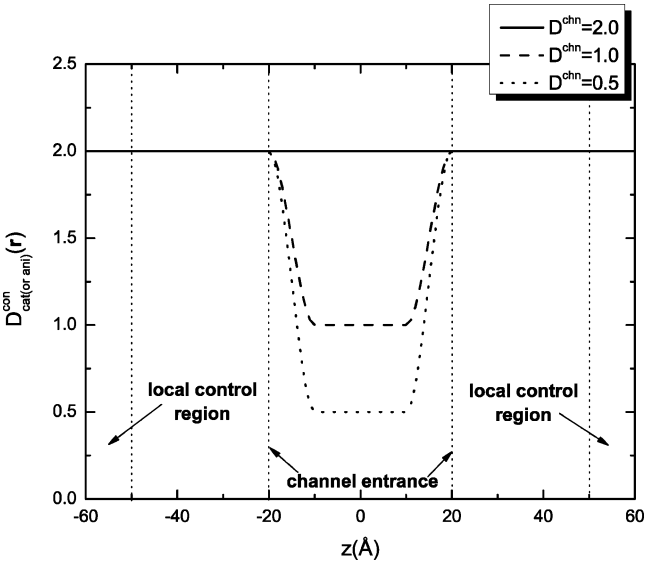

Figure 5. Continuously changing diffusion coefficients of ions as a function of *z*. The cation and anion are assumed to have the same bulk and inside-channel diffusion coefficients. The locations of the channel entrances at $z = \pm 20$ Å and the local control regions at $z = \pm 50$ Å are also shown. The diffusion coefficients are in units of 10^{-5} cm^2/s.

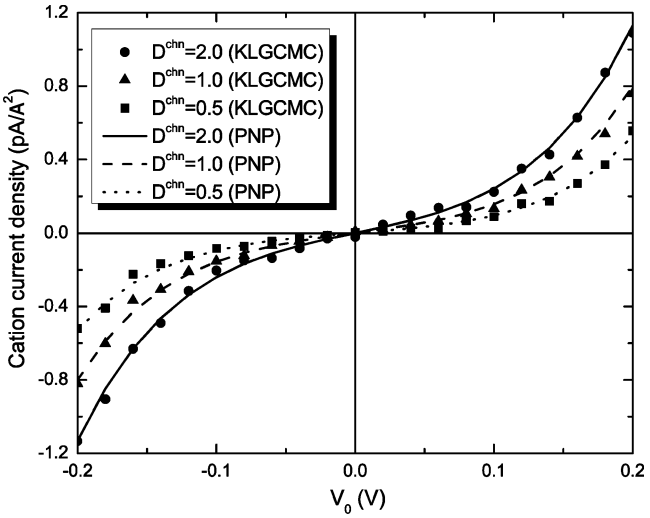

Figure 6. Dependence of cation current density−voltage curves on the inside-channel diffusion coefficients in the case of continuously changing diffusion coefficients. Comparison between the KLGCMC simulation results and the PNP calculations is also shown. For the same reason as in Figure 3, only the cation current densities are presented. The bulk salt concentration is 0.1 M. The diffusion coefficients (see inset) are in units of 10^{-5} cm^2/s.

$$D_{\text{cat(or ani)}}(\mathbf{r}) = \begin{cases} D^{\text{blk,top}}_{\text{cat(or ani)}} & z \geq L_{\text{chn}}/2, \\ D^{\text{chn,upp}}_{\text{cat(or ani)}} + (D^{\text{chn,upp}}_{\text{cat(or ani)}} - D^{\text{chn,low}}_{\text{cat(or ani)}})g(z) & |z| < L_{\text{chn}}/2, \\ D^{\text{blk,bot}}_{\text{cat(or ani)}} & z \leq -L_{\text{chn}}/2 \end{cases}$$

where $g(z) = (z/L_{\text{chn}} - 1/2)$. For the cation diffusion coefficient, $D^{\text{blk,top}}_{\text{cat}} = 1.5 \times 10^{-5}$ cm^2/s, $D^{\text{blk,bot}}_{\text{cat}} = 2.0 \times 10^{-5}$ cm^2/s, $D^{\text{chn,upp}}_{\text{cat}} = 1.0 \times 10^{-5}$ cm^2/s, and $D^{\text{chn,low}}_{\text{cat}} = 1.5 \times 10^{-5}$ cm^2/s, and for the anion diffusion coefficient, $D^{\text{blk,top}}_{\text{ani}} = 1.0 \times 10^{-5}$ cm^2/s, $D^{\text{blk,bot}}_{\text{ani}} = 1.5 \times 10^{-5}$ cm^2/s, $D^{\text{chn,upp}}_{\text{ani}} = 0.5 \times 10^{-5}$ cm^2/s, and $D^{\text{chn,low}}_{\text{ani}} = 1.0 \times 10^{-5}$ cm^2/s. $D_{\text{cat}}(\mathbf{r})$ and $D_{\text{ani}}(\mathbf{r})$ as a function of *z* are shown in Figure 8. As $D^{\text{blk,bot}}_{\text{cat}} > D^{\text{blk,bot}}_{\text{ani}}$, $D^{\text{ref}} = D^{\text{blk,bot}}_{\text{cat}} = 2.0 \times 10^{-5}$ cm^2/s, and the diffusion probabilities for the cation and anion are written as

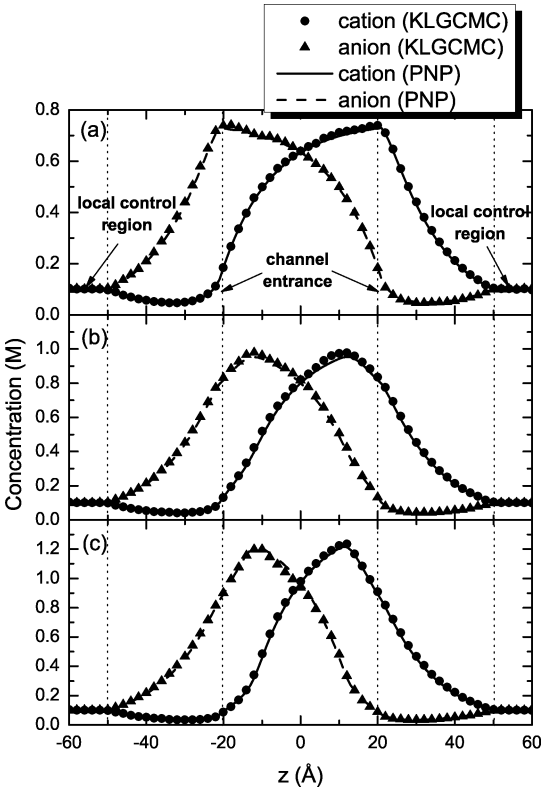

Figure 7. Dependence of cation and anion concentration profiles on the inside-channel ion diffusion coefficients at $V_0 = -0.2$ V. (a) $D^{\text{chn}} = 2.0 \times 10^{-5}$ cm^2/s, (b) $D^{\text{chn}} = 1.0 \times 10^{-5}$ cm^2/s, and (c) $D^{\text{chn}} = 0.5 \times 10^{-5}$ cm^2/s. Comparison between the KLGCMC simulation results and the PNP calculations is also presented. The locations of the channel entrances at $z = \pm 20$ Å and the local control regions at $z = \pm 50$ Å are also shown. The bulk salt concentration at both LC regions is 0.1 M.

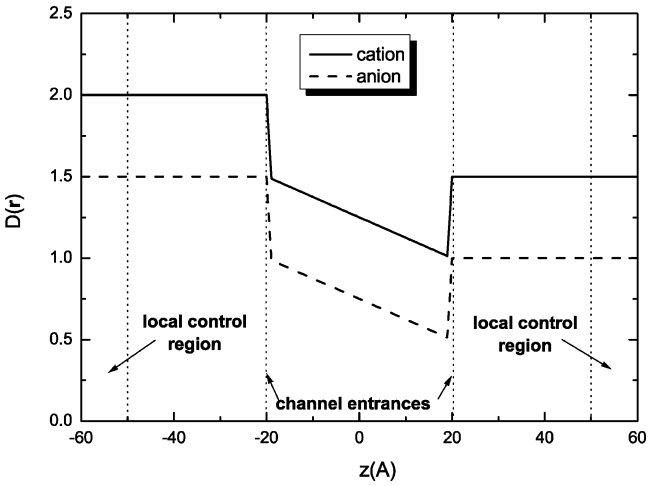

Figure 8. Asymmetric diffusion coefficients for the cation and anion as a function ofz. The location of the channel entrances at $z = \pm 20$ Å is shown. The diffusion coefficients are in units of 10^{-5} cm^2/s.

$$P^{\text{dif}}_{\text{cat(or ani)}}(\mathbf{r}) = \frac{D_{\text{cat(or ani)}}(\mathbf{r})}{D^{\text{ref}}} \tag{15}$$

Figure 9 shows the total, cation, and anion current density−voltage curves. The KLGCMC simulation results show good agreement with the PNP calculations. Due to the asymmetric diffusion coefficients of the ions in both baths and inside the channel, the current densities for the cation and anion are not symmetric with respect to $V_0 = 0$ V. However, note that the total current density−voltage curve is symmetric with respect

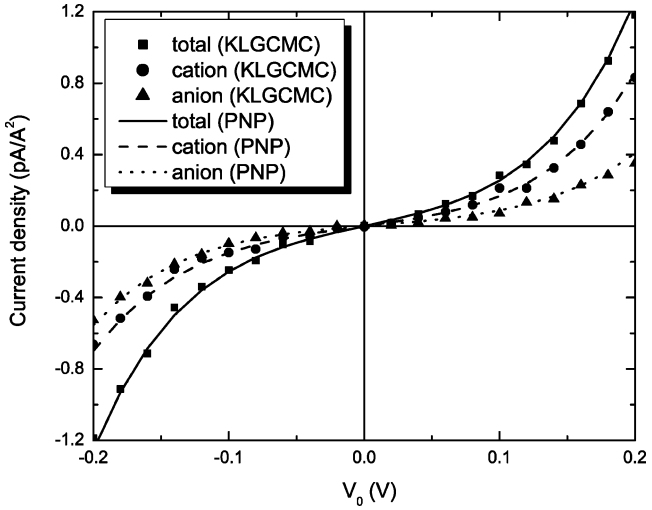

Figure 9. Total, cation, and anion current density−voltage curves when cations and anions have asymmetric diffusion coefficients in both baths as well as inside the channel. Comparison between the KLGCMC simulation results and the PNP calculations is also shown. The bulk salt concentration is 0.1 M.

to $V_0 = 0$ V. The higher diffusion coefficient of the cation than that of the anion in all the regions leads to the higher cation current densities than the anion current densities. There is no net current density for the cation or anion at $V_0 = 0$ V despite the asymmetric diffusion coefficients. It appears that at $V_0 = 0$ V, the decrease in cation diffusion coefficient along the channel axis (+z direction) causes downward movement of cations, which produces a negative current for the cation. However, due to the downward movement of cations, the cation concentration increases in the lower part of the channel. The increase in cation concentration in the lower part leads to a positive cation concentration gradient, which produces a positive current. As the result, the negative and positive currents cancel each other.

Cation and anion concentration profiles at $V_0 = -0.2$, 0, and 0.2 V are shown in panels a−c of Figures 10. At $V_0 = -0.2$ V, cations move downward and anions move upward. Because the diffusion coefficients of ions decrease along the channel axis (+z direction), anions move slower and pile up inside the channel more than cations. On the contrary, the concentration of cations increases inside the channel at $V_0 = 0.2$ V. The cation concentration inside the channel at $V_0 = 0.2$ V is smaller than the anion concentration at $V_0 = -0.2$ V because the cation diffusion coefficient is larger than the anion diffusion coefficient inside channel and bath. In Figure 10c, there is no increase of cation or anion concentration inside the channel.

IV. Conclusions

In this paper, we have presented an algorithm to implement inhomogeneous ion diffusion coefficients into a KLGCMC simulation method and calculated ion currents in a simple model ion channel system using the KLGCMC simulation method equipped with this algorithm. Based on move probability, this algorithm does not require altering the lattice spacing and interpolating electrostatic potentials, and as a result, is easy to implement. In addition, this probability-based algorithm can be easily incorporated into more realistic KLGCMC simulation methods because it requires modifying few parts of those KLGCMC simulations. The examples indicate that this algorithm can be employed both for discontinuously or continuously changing ion diffusion coefficients and for asymmetric diffusion coefficients of cations and anions in bulk as well as inside the channel.

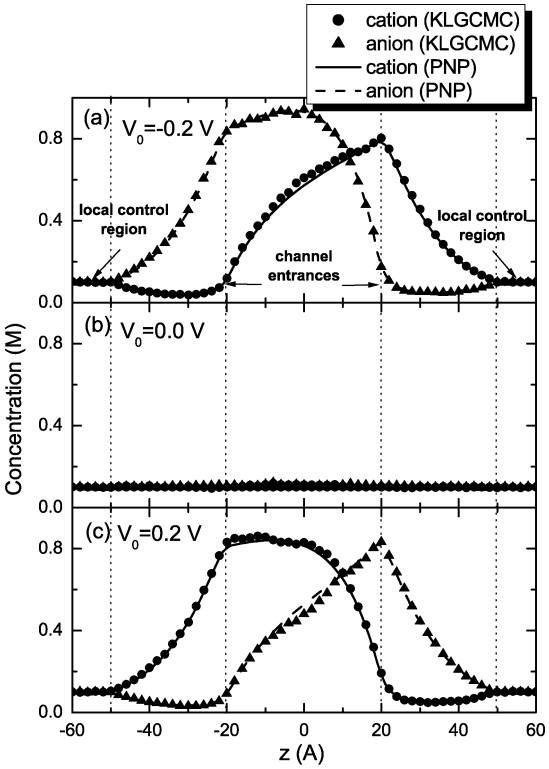

Figure 10. Cation and anion concentration profiles at $V_0 = -0.2$, 0.0, and 0.2 V. Comparison between the KLGCMC simulation results and the PNP calculations is also presented. The locations of the channel entrances at $z = \pm 20$ Å and the local control regions at $z = \pm 50$ Å are also shown. The bulk salt concentration at both LC regions is 0.1 M.

In the examples in this paper, a simple static field was used and fixed charges inside the channel were ignored. Also ignored is the reaction field effect which can play an important role in ion transport through an ion channel. Also, small ions were used to reduce finite size effects for the ions[33,34] and thereby to make it possible to test the KLGCMC method by comparison with PNP results for the same problem. The good agreement between results which we found indicates that the move probability algorithm is working correctly. In addition, the results provide insights concerning the influence of spatial anisotropy in the diffusion constant on the ion currents.

Combining this algorithm with a more realistic KLGCMC simulation method that we have previously developed,[4] provides a method that can be used for realistic ion channel problems where the inhomogeneous diffusion of ions inside the channel are important. This algorithm can also be used to describe the inhomogeneous diffusion of particles in other lattice-based simulations such as dip-pen nanolithography (DPN) simulations.[35,36]

Acknowledgment. This work was supported by the Network for Computational Nanotechnology (NCN) through a grant from the National Science Foundation, and by NSF Grant No. 0550497. H.H. is grateful to Prof. YounJoon Jung for a useful discussion.

References and Notes

(1) Graf, P.; Nitzan, A.; Kurnikova, M. G.; Coalson, R. D. *J. Phys. Chem. B* **2000**, *104*, 12324.

(2) van der Straaten, T.; Kathawala, G.; Ravaioli, U. *J. Comput. Electron.* **2003**, *2*, 231.

(3) Cheng, M. H.; Cascio, M.; Coalson, R. D. *Biophys. J.* **2005**, *89*, 1669.

(4) Hwang, H.; Schatz, G. C.; Ratner, M. A. *J. Chem. Phys.* **2007**, *127*, 024706.
(5) Corry, B.; Kuyucak, S.; Chung, S. H. *Biophys. J.* **2000**, *78*, 2364.
(6) Im, W.; Roux, B. *J. Mol. Biol.* **2002**, *322*, 851.
(7) Burykin, A.; Schutz, C. N.; Villa, J.; Warshel, A. *Proteins* **2002**, *47*, 265.
(8) Marreiro, D.; Tang, Y.; Aboud, S.; Jakobsson, E.; Saraniti, M. *J. Comput. Electron.* **2007**, *6*, 377.
(9) Hille, B. *Ionic Channels of Excitable Membranes*, 3rd ed.; Sinauer Associates, Inc.: Sunderland, MA, 2001.
(10) Jakobsson, E. *Methods* **1998**, *14*, 342.
(11) Roux, B. *Curr. Opin. Struct. Biol.* **2002**, *12*, 182.
(12) Eisenberg, B. *Biophys. Chem.* **2003**, *100*, 507.
(13) Smith, G. R.; Sansom, S. P. *Biophys. J.* **1998**, *75*, 2767.
(14) Warshel, A. *Acc. Chem. Res.* **2002**, *35*, 385.
(15) Allen, T. W.; Andersen, O. S.; Roux, B. *Proc. Natl. Acad. Sci. U.S.A.* **2004**, *101*, 117.
(16) Hwang, H.; Schatz, G. C.; Ratner, M. A. *J. Phys. Chem. B* **2006**, *110*, 26448.
(17) Chen, D.; Lear, J. D.; Eisenberg, R. S. *Biophys. J.* **1997**, *72*, 97.
(18) Kurnikova, M. G.; Coalson, R. D.; Graf, P.; Nitzan, A. *Biophys. J.* **1999**, *76*, 642.
(19) van der Straaten, T. A.; Tang, J.; Ravaioli, U.; Eisenberg, R. S.; Aluru, N. R. *J. Comput. Electron.* **2003**, *2*, 29.
(20) Hwang, H.; Schatz, G. C.; Ratner, M. A. *J. Phys. Chem. B* **2006**, *110*, 6999.
(21) Natori, A.; Godby, R. W. *Phys. Rev. B* **1993**, *47*, 15816.
(22) Righi, M. C.; Pignedoli, C. A.; Felice, R. D.; Bertoni, C. M. *Phys. Rev. B* **2005**, *71*, 075303.
(23) Oum, L.; Parrondo, J. M. R.; Martinez, H. L. *Phys. Rev. E* **2003**, *67*, 011106.
(24) Farnell, L.; Gibson, W. G. *J. Comput. Phys* **2005**, *208*, 253.
(25) Gillespie, D. *J. Phys. Chem.* **1977**, *81*, 2340.
(26) Fichthorn, K.; Weinberg, W. H. *J. Chem. Phys.* **1991**, *95*, 1090.
(27) Valleau, J. P.; Cohen, L. K. *J. Chem. Phys.* **1980**, *72*, 5935.
(28) Torrie, G. M.; Valleau, J. P. *J. Chem. Phys.* **1980**, *73*, 5807.
(29) Torrie, G. M.; Valleau, J. P. *J. Phys. Chem.* **1982**, *86*, 3251.
(30) Papadopoulou, A.; Becker, E. D.; Lupkowski, M.; van Swol, F. *J. Chem. Phys.* **1993**, *98*, 4897.
(31) Hoyles, M.; Kuyucak, S.; Chung, S.-H. *Phys. Rev. E* **1998**, *58*, 3654.
(32) Im, W.; Roux, B. *J. Chem. Phys.* **2001**, *115*, 4850.
(33) Gillespie, D.; Nonner, W.; Eisenberg, R. S. *Phys. Rev. E* **2003**, *68*, 031503.
(34) Gillespie, D.; Valisko, M.; Boda, D. *J. Phys. Condens. Matter* **2005**, *17*, 6609.
(35) Jang, J.; Hong, S.; Schatz, G. C.; Ratner, M. A. *J. Chem. Phys.* **2001**, *115*, 2721.
(36) Lee, N.-K.; Hong, S. *J. Chem. Phys.* **2006**, *124*, 114711.